INASS

International Journal of
Intelligent Engineering & Systems

http://www.inass.org/

Harmony Optimization Design of Switched Reluctance Motor Drive

Jie Li, Hexu Sun*, Zhaoming Lei

* *School of Electrical Engineering and Automation, Hebei University of Technology, Tianjin 300130, China*

* *Corresponding authors E-mail:hxsun@hebut.edu.cn*

Abstract: SRM has become an attractive alternative in adjustable speed drive due to its simplicity in both motor construction and power converter, and vibration that causes acoustic noise in SRM have generated intense interest from the time it became commercially competitive with dc and ac drives. Basically, there are two conventional ways to reduce the noise: optimize the physical structure of the motor, or, choose appropriate control strategies. In this paper, a new method is proposed to combine these two optimization ways together: harmony optimization of SRM. Physical design is mainly aiming at the back iron thickness and the air gap length of the motor. Control optimization is about the control mode, turn-on and the turn-off angle which affects the power factor strongly. Based on the same cooper losses, the mathematics analysis and finite element simulation are carried out. The results show that the harmony optimization will reduce the vibration and torque ripple in a large extent without extra power losses.

Keywords: SRM drive; optimization design; physical structure; control

1. Introduction

The switched reluctance motor (SRM) drives for industrial applications are of recent origin. Because of its simple structure and easy operation, the SRM can be an ideal alternative for other motors if its problems can be solved [1]. Serious acoustic noise caused by the torque ripple is still a primary reason for the SRM to be unacceptable in variable speed drive market [2]. Moreover, the construction of the SRM presents opportune circumstances to generate acoustic noise due to its specific magnetic configurations and manufacturing tolerances. The smallest air gap is designed to maximize torque and power output. Fewer poles, together with uneven machining or punching of diametrically opposite poles create uneven magnetic pull in the radial direction. Meanwhile acoustic noise problem is exacerbated. In addition to these manufacturing tolerances and magnetic shapes, converter and controller-related events, such as the drastic variation in rate of fall current in the machine phases by applying dc source voltage of negative polarity, results in immense radial vibrations. Negative voltage is applied to turn the faster current off to avoid generating torque of opposite polarity that is undesirable for the quadrant of operation of the SRM as it reduces the average torque. An understanding of many of these factors developed in the last few years led to many ameliorative measures in the design of the SRM and in its control [3-6]. Generally, there exist two ways to reduce the motor vibration and to eliminate the torque ripple: optimize the physical structure of the motor when designing the SRM; choose the appropriate control strategy. And, the conventional ways are always treated separately. The relationship between the motor's physical dimensions and excitation conditions is implicitly or not explicitly established [7,8]. In this paper, a new method is proposed to combine the two conventional optimization ways together, that is, a harmony optimization of SRM. The physical optimization is pri-

marily aiming at the back iron thickness b_s and the air gap length l_g. The relationships between back iron thickness and the motor's natural frequency, air gap length and the radial force are analyzed; the motor's output torque and the radial forces with variation dimension are simulated by using finite element software. And on the basis of these physical design analyses, control modes of the SRM including single phase excited, and the double phase excited and appropriate control strategy including the turn-on and turn-off angle are discussed under either the PWM operations or current limited control. The best switching point is selected with reference to a suitable motor dimension; it is approved that harmony optimization will reduce the vibration and torque ripple in a large extent without extra power losses. This work lays the foundation of designing higher performance of the SRM drive.

2. SRM physical dimension parametric analysis

The construction of the SRM presents opportune circumstances to generate acoustic noise due to its specific magnetic configurations and manufacturing tolerances. A qualitative design measures can be implemented at the design stage of SRM to reduce the noise effectively. The general optimization process adopted for SRM has been illustrated well by Tang [9] and is shown in Fig.1. And, the physical optimization design of switched reluctance machine has been attempted under the following categories: shape modification through choice of geometrical parameters; deterministic methods; soft computing methods.

Performance analysis of the SRM requires the dimensions for stator and rotor laminations, winding details, pole numbers, and pole arcs. An approximate sizing of the SRM is obtained using a power out put equation and the resulting machine dimensions form the starting point in optimization design analysis. Here, the dimension parametric analysis is employed and the performance of the prototype motor in finite element software Maxwell 2D package is calculated.

As the Static characteristics form the foundation of motor design, in order to obtain static magnetization characteristics, it is assumed that an ideal square current pulse applied, the motor's speed is sufficiently low and the SRM with one phase excited at any rotor position.

The entire excitation cycle is 60^{o} and the phase current conduction period is 30^{o}. The excitation sequence in the four-phase motor is shown in Fig. 2. Phase current pulse is used as abscissa; rotor position is used as

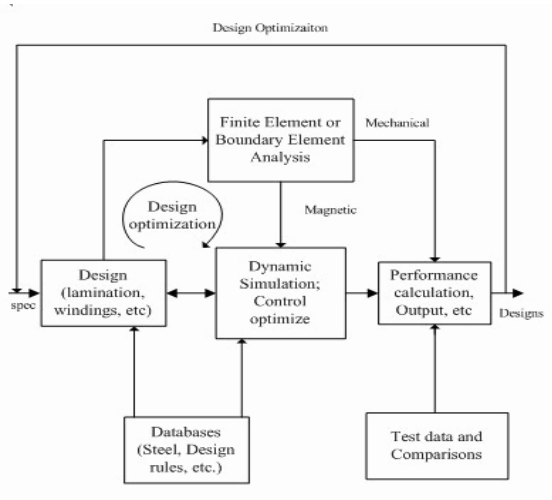

Figure 1. General design optimization process for SRM

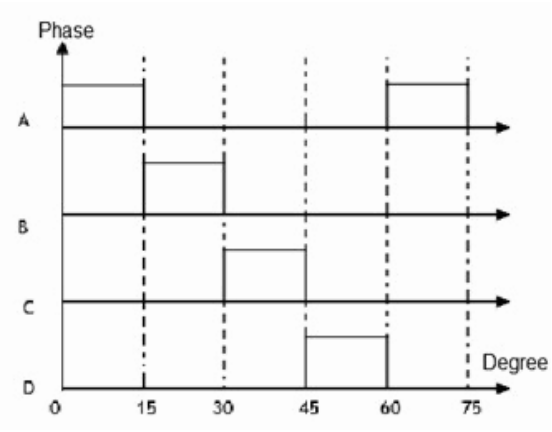

Figure 2. Excitation sequences in motor

coordinates [10].

The dimensions parameters discussed here are mainly about the back iron thickness b_s, air gap l_g, and other relevant dimensions including the stator outer diameter D_s, stator pole height H_s, rotor outer diameter γ, stator pole width ω_{sp}. The relevant dimensions of the SRM are shown in Fig. 3.

2.1 Back iron thickness parametric analysis

It is critical to know the frequencies at which various components of the radial force frequencies coincide with the natural frequency of the machine to generate resonance, leading to an increase in the acoustic noise. The stator of the machine has its own natural frequency. And similar to other machines, the SRM has radial forces producing vibrations that result in acoustic noise. This is mostly at the fundamental mode frequency of the SRM structure. If the phase frequency or its odd harmonics coincide with that of the SRM, then a resonance occurs, resulting in peak-

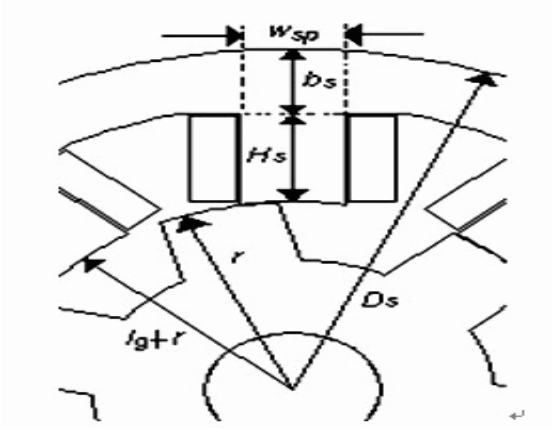

Figure 3. Relevant dimensions of the SRM

ing of stator vibration. The phase frequency is:

$$f_p = (\frac{\omega}{2\pi})P_r \tag{1}$$

Where ω_m is the speed in rads/sec and P_r is the number of rotor poles. Vibration is maximum if any of the frequencies,

$$f_n = nf_p, n = 1,3,5,7,... \tag{2}$$

are coincident with the natural frequency f of the stator. Vibrations seem to diminish for even harmonics of phase frequency coinciding with natural frequency f of the SRM structure. Then, to control the acoustic noise, the natural mode frequency of the motor has to be evaluated [11,12].

Assuming the stator lamination stack as a uniform cylindrical shell, whose thickness is b_s, that is the back iron thickness, and the stack length is L. When a vertical load w is applied on this ring structure, a deflection result makes the ring distort into an ellipse. Due to the load application, the potential energy must be equal to the kinetic energy arising out of the deflection for energy conservation of the structure. From this, the angular natural frequency can be obtained as:

$$\omega^2 = \frac{2}{12\pi(1-\gamma^2)(\frac{\pi}{4}-\frac{2}{\pi})}(\frac{E}{\rho})(\frac{b_s^2}{r_y^4}) \tag{3}$$

where γ is the poisson ratio, ρ is the mass density of the material, γ_y is the geometric mean radius of the stator shell, E is the modulus of elasticity [13,14].

From Eqs.(1) and (3), it can be seen that the fundamental mode frequency is primarily influenced by back iron thickness and to a lesser extent by the outer diameter of the stator lamination. For that, when we design a SRM, the outer diameter of the motor is always a constant for a given power and speed in industrial production. This leaves the back iron thickness as an important design parameter.

From Eq.(3), it is obvious that a higher thickness is favorable as it increases the first mode frequency, thus the resonance which results in peaking of stator vibration can be avoid effectively. Also, a higher thickness gives higher mechanical strength which restrains the stator's distortion caused by the radial force. The penalty of a higher thickness then is a large back iron thickness that increases the weight, current density and copper losses but reduces the available area for windings. In the design process a tradeoff has to be achieved. The stator back iron thickness b_s is based on the maximum flux density in it and by the additional factor of vibration minimization to reduce acoustic noise. Always, b_s has a value in the range of:

$$\omega_s p > b_s \geq 0.5\omega_s p \tag{4}$$

To dig the relationship between the back iron thickness and output performance of a SRM, a finite element model of the prototype motor is created in Maxwell 2D package. The motor's specifications are given in Table 1.

Table 1. Specifications of SRM prototype

Item	Prototype
No. of phase	4
No. of stator/rotor poles	8/6
Stator outer diameter[mm]	145
Rotor outer diameter[mm]	79.5
Back iron thickness[mm]	14
Stator pole arc[degree]	21
Rotor pole are[degree]	24
Air-gap length[mm]	0.25
Winding (turns per pole)	72
Rated torque (N.m)	7

The motor is excited in one phase current conduction period 30^o with an ideal square current pulse as seen in Fig.2. The back iron thickness of the motor is varied from ω_{sp} to $0.5\omega_{sp}$ with an equal interval of 2mm. This variation of back iron thickness results in a corresponding change in the stator pole height while there are enough space for the winding arrangement. Other parameters of the motor are held constant.

Fig.4. is the parametric analysis setup in the software, where the initial dimension of the b_s is 14mm. And with an equal interval of 2mm, b_s changes from 14mm to 7mm. Fig.5. is the family curves of output

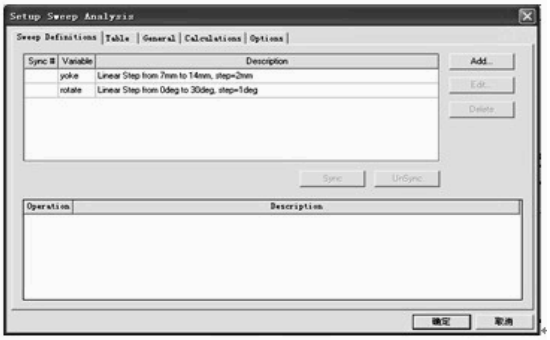

Figure 4. Parametric analysis setup

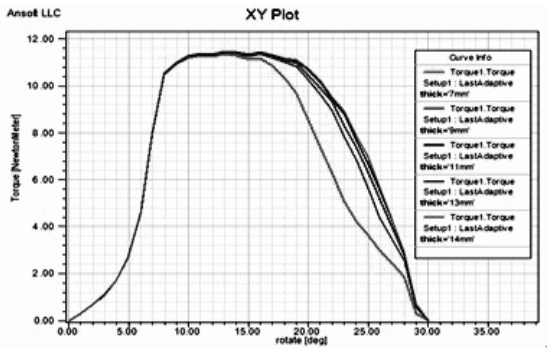

Figure 5. Static torque versus rotor position curves

torque with different back iron thickness, where the simulation result illustrates that a bigger b_s tends to increase the motor's output and that the b_s not only affects the torque output but also controls the shape of the static torque profile. A curve colors red has a departure when the stator back iron thickness b_s is too small thus the stator yoke is heavily saturated. In this case a flatter torque versus angle characteristic may be achieved by compromising the back iron thickness.

2.2 Air gap length parametric analysis

Air gap length is an important design parameter of SRM. The magnetic flux in the machine passes across the air gap in an approximate radial direction producing radial forces on the stator and rotor, resulting in magnetic noise and vibrations. The radial forces in the SRM are directly proportional to the square of the flux density in the air gap, assuming that the iron is infinitely permeable and has zero reluctance which leaves only the air gap to provide reluctance in the circuit.

The air gap flux density at a given stator and rotor pole overlap angle θ, air gap lg, and current i is given as

$$b_g(\theta, l_g, i)$$

. Let r be the outer radius of the rotor, L be the stack length or iron length in the z direction, Tph be the number of turns in one phase of the machine, i be the current in the winding, Hg be the magnetic field strength, Φ be the flux, and μ_0 be the permeability of air, then the variables are derived as:

$$B_g(\theta, l_g, i) = \frac{\Phi}{Lr\theta} = \mu_0 H_g = \mu_0 \frac{T_{ph} i}{l_g} \tag{5}$$

$$T_{ph} i = \frac{l_g}{\mu_0 Lr} \frac{\Phi}{\theta} \tag{6}$$

The incremental electrical input energy dWe is given by:

$$dw_e = id\lambda = id(T_{ph}\Phi) = T_{ph} id\Phi = \frac{l_g}{\mu_0 Lr} \frac{\Phi}{\theta} d\Phi \tag{7}$$

The stored energy in the magnetic field dWs is

$$W_s = \frac{l_g Lr\theta}{2\mu_0} B_g^2(\theta, l_g.i) = \frac{l_g}{2\mu_0 rL} \frac{\Phi^2}{\theta} \tag{8}$$

where the term $l_g Lr\theta$ gives the volume of the air gap contained by the stator and rotor pole overlap. Note that $r\theta$ gives the arc of the overlapping region between the stator and rotor poles. The energy balance equation neglecting losses is:

$$dW_e = dW_s + dW_m \tag{9}$$

where dWm is the incremental mechanical energy and dWs is the incremental field energy. To find the tangential, radial, and lateral forces, note that the incremental field energy for that directional variable has to be taken and substituted in Eq.(9). As the electrical input energy is given in Eq.(7), the mechanical energy is computed by subtracting the incremental field energy from the incremental input energy [15-17].

The incremental field energy is obtained from Eq.(8) as:

$$dW_s = \frac{l_g}{2\mu_0 Lr} \frac{\Phi^2}{\theta^2} d\theta + \frac{l_g}{\mu_0 Lr} \frac{\Phi}{\theta} d\Phi \tag{10}$$

The second term on the right side of Eq.(10) is based on the fact that Φ is the air gap flux density and that it is a function of rotor position, l_g and i.

Substitute Eqs.(7) and (10) in Eq.(9), the incremental mechanical energy is obtained as:

$$dW_m = \frac{l_g}{2\mu_0 Lr} \frac{\Phi^2}{\theta^2} d\theta \tag{11}$$

Then the tangential torque is obtained as:

$$T_e = \frac{dW_m}{d\theta} = \frac{l_g}{2\mu_0 Lr}\frac{\Phi^2}{\theta^2} = \frac{l_g rL}{2\mu_0}B_g^2(\theta, l_g, i) \quad (12)$$

Therefore, the tangential force is obtained by dividing the tangential torque by the radius of the rotor pole, yielding:

$$F_t = \frac{T_e}{r} = \frac{l_g L}{2\mu_0}B_g^2(\theta, l_g, i) \quad (13)$$

The radial force in the direction of the air gap is obtained from considering the incremental field energy with respect to the air gap and the incremental mechanical energy as:

$$dW_m = -\frac{1}{2\mu_0 rL}\frac{\Phi^2}{\theta}dl_g \quad (14)$$

and the radial force is :

$$F_n = \frac{dW_m}{dl_g} = -\frac{1}{2\mu_0}.\frac{\Phi}{\theta} = -\frac{r\mu_0 L\theta.T_{ph}^2.i^2}{2l_g^2} \quad (15)$$

Similarly, the lateral force can be derived as:

$$F_y = \frac{l_g r\theta}{2\mu_0}B_g^2(\theta, l_g, i) \quad (16)$$

From the equations above, it can be stated that lateral force and tangential force are of similar magnitude but the radial force is not. From Eqs.(13) and (15), the ratio between the radial force and tangential force is:

$$\frac{F_n}{F_t} = -\frac{r\theta}{l_g} \quad (17)$$

The rotor angle can be assumed to be equal to the one-phase conduction angle which in terms of the rotor and stator poles is given as:

$$\theta = \frac{4\pi}{P_s P_r} \quad (18)$$

where P_S and P_r are the number of stator and rotor poles.

From the analytical expression, an obvious way to reduce noise would be to reduce the flux density by enlarging the air gap. Also a larger air gap is preferred from the manufacturing points of view. It is clear that a large air gap length is preferred in a reasonable range.

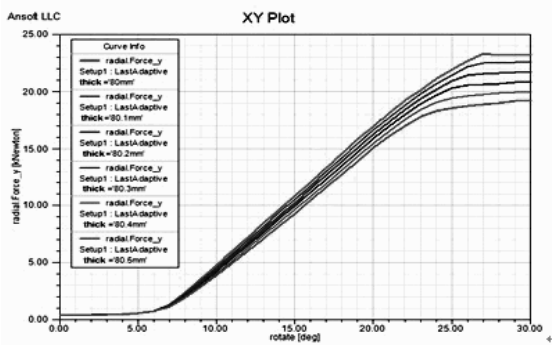

Figure 6. Radial forces versus rotor position curves

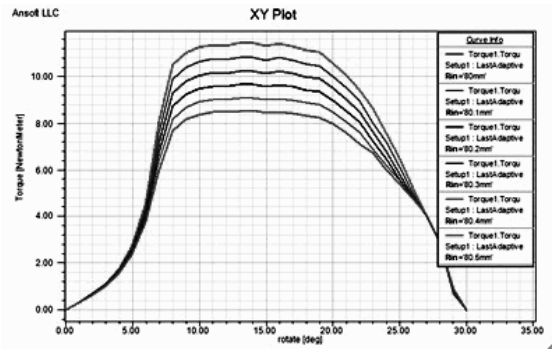

Figure 7. Static torque versus rotor position curves

Again, a finite element model of the prototype motor is created in Maxwell 2D package. The specification of the motor is given in Table 1. In one conduction period 30^o, the ideal square current pulse is applied to one phase winding. The motor's radial force and the output torque with a series air gap value are calculated with the same current.

Considering the mechanical robustness and the minimization of vibration, the air gap could have a value in the range of 0.25 to 0.5. Fig.6 and Fig.7 are the family curves of radial forces and the output torque with variation of air gaps.

Fig. 6 is the family curves of radial forces versus rotor position. It can be seen that radial force is a large magnitude value of thousands Newton. As the air gap increases from 0.25mm to 0.5mm, the radial force reduces from 23.3kN.m to 19.2KN.m. The drop of radial force gradually grows as the rotor pole rotates to the aligned position. At the aligned position particularly, the motor with a 0.5mm air gap could reduce 400N.m (almost 20%) radial force compared with a 0.25mm air gap length. In this way, the stator's distortion can be mitigated effectively. But notice that the smallest air gap can maximize the torque and the power output of the motor. Fig.7 compares the static torque produced by the motor with different

air gap length. The static torque rises from 8.2N.m to 10.8N.m when air gap decreases from 0.5mm to 0.25mm. In this case, it is necessary to make a trade-off according to the practical needs.

3. Harmony optimization of physical design and control strategy of SRM

Conventional control category of the SRM is either the single phase excited mode or the double phase excited mode under either the PWM operations or current limited control [18]. The double phase excited mode is always used in the odd phase circuit. Comparing with the single phase excited mode, the advantage of the double phase excited mode can make a significant improvement in torque production and a reduction in torque ripple to the motor. But considering the commutation freewheeling of current in the windings, part of the electrifying windings produce a negative torque, thus the complexity of controlling loops increases [19][20]. Besides, as the rotor poles rotate to the aligned position, the high flux density in the iron will bring a significant impact on the motor: increase the motor losses and reduce the efficiency. Here, an improved double excited mode is presented which can be applied to any type of the SRM, that is, a mix-excited mode.

It is known that vibration is much nearer to the aligned position comparing with the unaligned position. Turning off before full alignment reduces vibrations. And by commutating the current before alignment, the deeply saturated stator yoke is relieved magnetically. It's better to make a turn-off before full alignment under double phase excited working mode.

Based on the analysis in the previous section, the choice of appropriate back iron thickness and air gap with a good switching point under double phase excited working mode can extend the flat torque period and reduce the core loss. A four-phased 8/6 SRM with optimized structure working under different control mode is simulated for harmony optimization. The results of the motor's output performance are compared in Fig. 8, Fig. 9 and Fig. 10.

As shown in Fig. 8, Fig. 9, Fig. 10, the red line is the performance of one phase excited working mode with the initial motor structure, the green line is the performance of two phases excited working mode with the initial motor structure, and the blue line is the mix-excited working mode with an optimization motor structure.

The harmony optimization process is: optimize the physical structure of the motor, especially aiming at

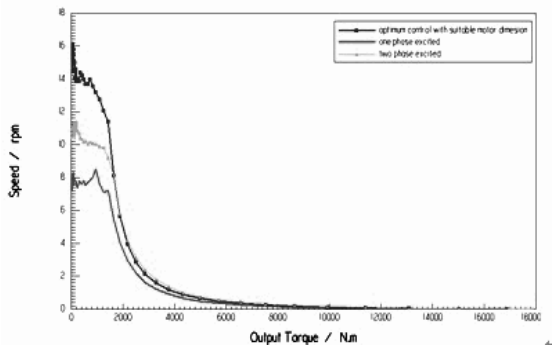

Figure 8. Output torque versus speed

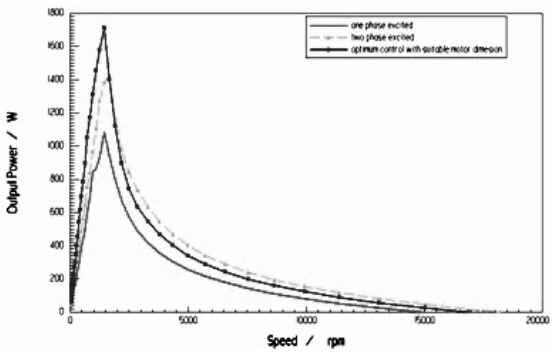

Figure 9. Output power versus speed

the air gap and back iron thickness; calculate the flux density of the aligned position with double excited mode and choose an advanced switching point based on the iron material properties point which can avoid the saturation in the iron of the yoke.

It can be seen that by enlarging the air gap length to 0.35mm and the back iron thickness to 15mm, operating the machine at an optimum switching point of 22^o with the same excitation current under mix-excite mode, both the output torque and the output power have greatly increased. And when the motor is operated below 8000rpm, the optimized motor has the highest efficiency. In a practical motor, if a photoelec-

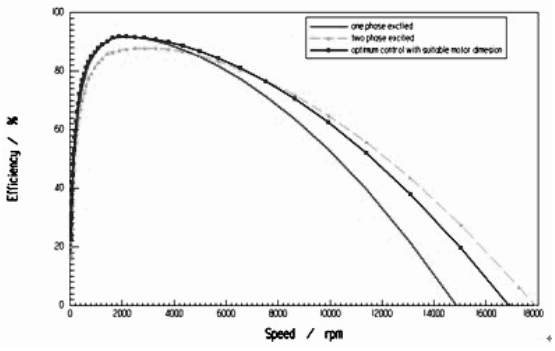

Figure 10. Efficiency versus speed

tric encoder position feedback arrangement is used, a precise tiny angle resolution could be available to have the accurate switching point.

4. Conclusion

This paper presents a new method to optimize the SRM: a harmony optimization method which combines the physical dimension design and control strategy together. Detailed investigations and simulations have been carried out to analyze the relationships between dimensions and the motor's output performance. Especially, discussions are focused on the air gap and the back iron thickness. It is approved that a smooth torque characteristic can be achieved by careful selection of the motor's back iron thickness, and that the radial force of the motor can be greatly reduced if the air gap is perfect. By analyzing the different control mode, the best switching point is selected with reference to the suitable motor dimension. The simulation shows that the choice of appropriate stator back iron thickness and air gap length coupled with perfect switching point will not only reduce the vibration and torque ripple to a large extent but also improve the motor's output performance without extra power losses. Comparing mix-excited mode with the single phase excited mode, the starting torque has increased 70%, the rated torque has increased 100%, and the output power has increased 60% at the rated speed. When the speed is less than 3800rpm, both efficiencies are equal; when the speed goes up to 3800rpm, the mix-excited mode exceeds. Comparing mix-excited mode with double excited mode, the starting torque has increased 36%, the rated torque has increased 10%, and the output power has increased 20% at the rated speed. And below 7000rpm, the efficiency of the motor under mix-excited working mode is much higher. Note that all the simulations above are based on the same winding current.

It is verified that the SRM performance can be improved efficiently. This method discussed in this paper lays the foundation of designing higher performance of SRM and its significant value symbolizes the real meaning of innovation.

5. Acknowledgments

The authors gratefully acknowledge financial support from National High Technology Research and Development 863 Program of China under Grant Number 2006AA040306.

References

[1] Timar and P.L., *Noise and Vibration of Electrical Machines*, Elsevier, Amsterdam/New York, 1989.

[2] Wu, C.Y. and C. Pollock, "Analysis and reduction of vibration and acoustic noise in the switched reluctance drive ", *Conf. Record, IEEE IAS Ann. Mtg.*, 93CH3366-2, pp.106-113, 1993.

[3] Lisner, R. and L. Timar, "A new approach to electric motor acoustic noise standards and test procedures", *in IEEE Int. Electric Machines and Drives Conf. Rec.*, Milwaukee, WI, pp. 6.1-6.3, 1997.

[4] R.Krishnan, *SRM Drives: Modeling, Simulation, Analysis, Design and Application*, CRC Press LLC, Florida, 2001.

[5] Beno, M.Marsaline, Marimuthu, N.S., Singh, N. Albert. "Improving power factor in SRM drive system by optimizing the switching angles", *IEEE Region 10 Annual International Conference*, Proceedings/TENCON 2008.

[6] S.-H. Mao and M.-C. Tsai, "An analysis of the optimum operating point for a SRM," *J. Magn. Magn. Mater.*, vol. 282, pp.53-56, 2004.

[7] J. P. Hong, K. H. Ha, and J. Lee, "Stator pole and yoke design for vibration reduction of SRM," *IEEE Trans. Magn.*, vol. 38, no. 2, pp. 929-932, Mar. 2002.

[8] J. W. Ahn, S. J. Park, and D. H. Lee, "Hybrid excitation of SRM for reduction of vibration and acoustic noise," *IEEE Trans. Ind. Elect.*, vol.51, no. 2, pp. 374-380, Apr. 2004.

[9] Y.Tang and F.A Kline, "Modeling and design optimization of switched reluctance machine by boundary element analysis and simulation," *IEEE Trans. Energy Convers.*, Vol.11, no. 4, pp. 673-680, Dec.1996.

[10] Jie Li, Hexu Sun, "Modeling and simulation of four-phase 8/6 SRM with an improved winding configuration", *Proceedings of International Conference on Computer Science and Software Engineering, CSSE 2008*, v 4, pp. 1045-1048.

[11] Singal, R.K., K. Williams, and S.P. Verma, "The effect of windings, frame and impregnation upon the resonant frequencies and vibrational behavior of an electrical machine stator," *Experimental Mechanics*, 30, 270-280, 1990.

[12] Vijayraghavan, P. and R. Krishnan, "Noise in electric machines: a review," *IEEE Trans. on Ind. Appl.*, Vol. 35, No. 5, pp. 1007-1013, Sept. Oct., 1999.

[13] Kim, K.-B., "Field analysis of low acoustic noise SRM", *IEEE Trans. on Magnetics*, 33(2), pp. 2026-2029, 1997.

[14] Cameron, D.E., J.H. Lang, and S.D. Umans, "The origin and reduction of acoustic noise in doubly salient variable-reluctance motors", *in IEEE Trans. on Ind. Appl.*,28(6), 1250-1255, 1992.

[15] Colby, R.S., F.M. Mottier, and T.J.E. Miller, "Vibration modes and acoustic noise in a four-phase SRM," *in IEEE Trans. on Ind. Appl.*, 32(6), 1357-1364, 1996.

[16] S. Ayari, M. Besbes, M. Lecrivain, and M. Gabsi, "Effects of the airgap eccentricity on the SRM vibrations," *in Proc. IEEE Electric Machines and Drives Conf.*, 1999, pp. 138-140.

[17] N. K. Sheth and K. R. Rajagopal, "Variations on overall developed torque of a SRM with airgap nonuniformity," *IEEE Trans. Magn.*, vol. 41, no. 10, pp. 3973-3975, Oct. 2005.

[18] Stemmler, H. and T. Eilinger, "Spectral analysis of the sinusoidal PWM with variable switching frequency for noise reduction in inverter-fed induction motors", *in Proc. 1994 Power Electronics Specialist Conf.-PESC '94*, Vol. 1, Taipei, Taiwan, 1994, pp. 269-277.

[19] Chen, G.H., Tseng, K.J. "Design of wheel motor using Maxwell 2D simulation", *Proceedings of the International Conference on Energy Management and Power Delivery, EMPD, Singapore*, 1995, pp. 634-639.

[20] R.Krishnan, *SRM Drives: Modeling, Simulation, Analysis, Design and Application*, CRC Press LLC, Florida, 2001.

[21] J. W. Ahn, S. J. Park, and D. H. Lee, "Hybrid excitation of SRM for reduction of vibration and acoustic noise," *IEEE Trans. Ind. Elect.*, vol. 51, no. 2, pp. 374-380, Apr. 2004.

[22] P. Rfajdus, I. Zrak, and V. Hrabovova, "Analysis of the SRM (SRM) parameters," *J. Elect. Eng.*, vol. 55, no. 7-8, pp. 195-200, 2004.

[23] N. K. Sheth and K. R. Rajagopal, "Variations on overall developed torque of a SRM with airgap nonuniformity," *IEEE Trans. Magn.*, vol. 41, no. 10, pp. 3973-3975, Oct. 2005.

[24] Zhang Hai-Jun, Gao Rui-zhen, Zhang Jing-Jun, "Control simulation for SRM system based on finite element model", *Meitan Xuebao/Journal of the China Coal Society*, v 33, n 7, pp. 831-836, July 2008.

[25] B. Parreira, S. Rafael, A. J. Pires, and P. J. Costa Branco, "Obtaining the magnetic characteristics of an 8/6 switched reluctance machine: From FEM analysis to the experimental tests," *IEEE Trans. Ind. Appl.*, vol. 52, no. 6, pp. 1635-1643, Dec. 2005.